Electroless Pt Deposition on Mn_3O_4 Nanoparticles *via* the Galvanic Replacement Process: Electrocatalytic Nanocomposite with Enhanced Performance for Oxygen Reduction Reaction

Ki Woong Kim,[†,⊥] Soo Min Kim,[‡,⊥] Suhee Choi,[§] Jongwon Kim,[§,*] and In Su Lee[‡,*]

[†]Department of Applied Chemistry, Kyung Hee University, Gyeonggi-do 446-701, Korea, [‡]Department of Chemistry, Pohang University of Science and Technology (POSTECH), Gyeogbuk 790-784, Korea, and [§]Department of Chemistry, Chungbuk National University, Chungbuk 361-763, Korea. [⊥]These authors contributed equally to this work.

ABSTRACT

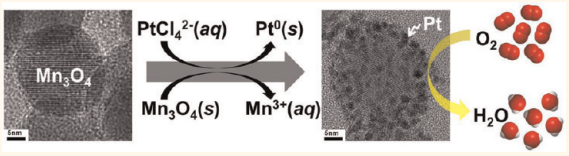

A novel electroless Pt deposition method was exploited by employing the galvanic replacement process occurring between the Mn_3O_4 surface and $PtCl_4^{2-}$ complexes. The newly discovered process provides a simple protocol to produce the catalytic nanocomposite, in which a high density of ultrafine Pt nanocrystals is stably immobilized in a homogeneously dispersive state on the surface of Mn_3O_4 nanoparticles. When the eletrocatalytic activity was tested for the oxygen reduction reaction, which limits the rate of the overall process in proton-exchange membrane fuel cells, the resulting Pt/Mn_3O_4 nanocomposite showed highly enhanced specific activity and durability, compared with those of the commercial Pt/C catalyst.

KEYWORDS: nanoparticles · manganese · platinum · electroless deposition · electrocatalysis

Over the past several decades, considerable attention has been focused on using metal nanoparticles for developing effective catalytic materials.[1,2] As the particle size decreases, a larger fraction of active metal atoms are exposed to the surface, and thus ultrafine nanoparticles often exhibit highly enhanced catalytic activities. On the other hand, the high surface energy of the nanoparticles results in sintering or coalescence, causing a serious decline in their performance during catalytic operation and hence impeding their use in industrial processes. One of the effective strategies for circumventing such a deactivation problem is the use of proper support materials that can stabilize the dispersed state of the nanoparticles against the sintering process.[3,4] Because of their large surface area, high binding affinity to metal species, and superior stability against thermal, mechanical, and oxidative stresses, metal oxide nanoparticles are attractive candidates as solid supports for nanocatalytic systems.[5−7] In addition, the synergetic effect at the metal/metal oxide heterojunction occasionally leads to considerably improved catalytic performance which cannot be achieved with unsupported catalysts.[8−10]

While studying metal-oxide-supported catalytic systems, we discovered spontaneous growth of Pt on the surface of Mn_3O_4 particles from a suspension containing Pt^{2+} complexes *via* unexpected electroless processes that did not require any additional reducing agents. This is a unique and interesting phenomenon involving a galvanic replacement reaction which has only rarely been observed between metal oxides and metal ions.[11−17] In addition to providing fundamental knowledge, the discovered Pt growth process also allows the simple and efficient deposition of catalytic nanocrystals on a metal oxide support with high surface area, which can be useful for developing supported catalyst systems with optimized performance.[18−21] In this paper, we report the high density deposition of ultrafine Pt nanocrystals on the surface of Mn_3O_4 nanoparticles while simultaneously preserving the dispersed state *via* a spontaneous and electroless process. In order to identify the

* Address correspondence to jongwonkim@chungbuk.ac.kr, insulee97@postech.ac.kr.

Received for review February 21, 2012 and accepted May 3, 2012.

Published online May 11, 2012
10.1021/nn300782m

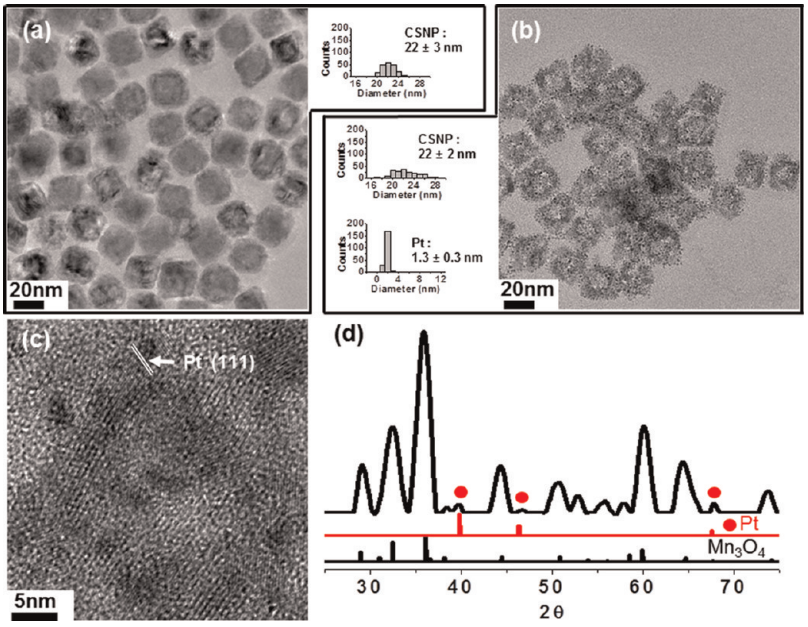

Figure 1. (a) TEM and size distribution histogram of CSNPs. (b) TEM and size distribution histograms, (c) HRTEM, and (d) XRD pattern of nanoparticles obtained by treating CSNPs in a Na_2PtCl_4 solution (7.5 mg/mL) at 70 °C for 30 min. XRD peaks corresponding to Pt are marked with red circles. The lines below show the position of the reflections corresponding to tetragonal Mn_3O_4 phase (JCPDS Card No. 24-0734) and the fcc Pt phase (JCPDS Card No. 87-0646).

potential utility in the catalytic application, the electrocatalytic activity of the resulting Pt/Mn_3O_4 nanocomposite was tested for the oxygen reduction reaction (ORR) as a model reaction. We also report the highly enhanced specific catalytic activity and durability of the synthesized catalytic nanocomposite in the ORR over commercial Pt/C catalysts.

RESULTS AND DISCUSSION

Spontaneous Growth of Pt Nanocrystals on the MnO−Mn_3O_4 Core−Shell Nanoparticle. The spontaneous Pt growth was first observed in the course of our efforts to immobilize Pt nanocrystals on the polyethyleneglycol (PEG)-coated MnO−Mn_3O_4 core−shell nanoparticles (CSNPs) prepared through a previously reported procedure.[22,23] When a Na_2PtCl_4 solution (7.5 mg/mL) was added to an aqueous suspension of 22 (±3) nm-sized CSNPs with gentle stirring at 70 °C, the color of the suspension gradually darkened and a translucent dark-brown suspension was generated within 30 min. Transmission electron microscopy (TEM), high-resolution TEM (HRTEM), and X-ray diffraction (XRD) of the resulting solids revealed the formation of tiny Pt nanocrystals averaging 1.3 (±0.3) nm in size on the surface of the Mn_3O_4 nanoparticles (Figure 1). It was also revealed that the MnO core in the CSNPs was selectively dissolved, most likely because of the acidic condition at pH 4.0, as already observed in our previous study.[23] The dissolution of MnO left a hollow Mn_3O_4 nanoshell decorated by multiple numbers of tiny Pt nanocrystals. A longer reaction time resulted in the deposition of higher number of Pt nanocrystals with slightly increased sizes of 1.3 (±0.3) and 1.7 (±0.3) nm at 60 and 120 min, respectively (Figure S1 in the Supporting Information). The experiment at room temperature did not allow any reaction between CSNPs and $PtCl_4^{2-}$. When $PtCl_4^{2-}$ was treated with $MnCl_2$ solutions or supernatant solutions obtained by centrifuging the hollow Mn_3O_4 nanoparticles after etching CSNPs in a HCl solution as a control, the formation of any metallic Pt was not detected. This indicates that the Mn_3O_4 part that remained after etching of the MnO cores is responsible for the Pt growth process. This Pt growth process differs from the traditional metal deposition method, which requires additional reduction sources.[24]

High Density Deposition of Pt Nanocrystals on the Surfactant-Free Mn_3O_4 Nanopareticle: Formation of Pt/Mn_3O_4 Nanocomposite. To better understand this process, we investigated possible Pt growth on Mn_3O_4 nanoparticles without any surfactant coatings on the surface. The use of surfactant-free Mn_3O_4 nanoparticles would exclude any influence of the organic shell and thus enable us to identify the contribution of the Mn_3O_4 surface to the spontaneous Pt growth. The surfactant-free Mn_3O_4 nanoparticles (Sf-MONs) were prepared through the solid-state transformation procedure within silica nanospheres, which includes the successive steps of coating oleic-acid-stabilized MnO nanocrystals with a silica shell, transforming MnO nanocrystals into Mn_3O_4, calcining the organic substance at high temperature, and etching the silica shell with a basic aqueous solution (Scheme 1).[25,26] The formation of the targeted Sf-MONs with a size of 21 (±1) nm was verified by TEM, HRTEM, and XRD (Figures 2a and 3). When Sf-MONs were

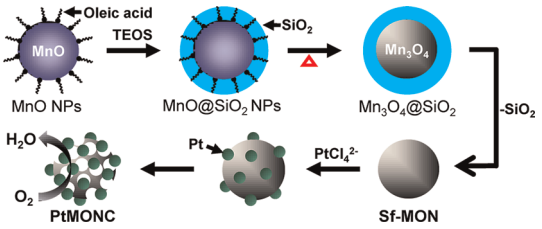

Scheme 1. Preparation of Sf-MON and PtMONC.

immersed in an aqueous solution of Na_2PtCl_4 at 70 °C, Pt nanocrystals were spontaneously formed on the Sf-MON surface, which confirmed the involvement of an intact Mn_3O_4 surface in the Pt growth process. TEM images obtained after a reaction time of 30 min show the generation of the core−satellite structure, where multiple numbers of tiny Pt nanocrystals averaging 1.6 (±0.3) nm in size are attached to the spherical surface of the Sf-MONs (Figure 2b). Longer reaction times cause additional nucleation and consequently additional deposition of Pt nanocrystals with slightly larger particle sizes. Another observation is that the Mn_3O_4 was slowly but gradually dissolved during the reaction. The TEM images at different reaction times reveal that the Sf-MONs become more porous as the reaction proceeds, indicating that the Pt deposition and Mn_3O_4 dissolution are interrelated and simultaneously progress along with the reaction time. The formation of a metallic Pt species accompanied by Mn_3O_4 dissolution was also confirmed by HRTEM and XRD analysis (Figures 2 and 3). Therefore, the TEM image obtained after a reaction time of 4 h shows the generation of a Pt/Mn_3O_4 nanocomposite (PtMONC) in which 2.3 (±0.4) nm-sized Pt nanocrystals are densely and uniformly dispersed at the porous surface of the Mn_3O_4 nanoparticles (Figure 2e). After a reaction time of 14 h, the nanoparticulate structure of the Sf-MONs collapsed and some Pt nanocrystals were sintered into larger grains (Figure 2f). When the Sf-MONs were treated in HCl solutions as a control, no dissolution was detected, which indicates that the observed Mn_3O_4 dissolution was caused by the reaction with Na_2PtCl_4. The elemental analysis of the solid samples isolated from reaction suspensions at different time also provides evidence that the Pt growth proceeded at the expense of Mn_3O_4 which served as a sacrificial template (Table S1). Similar to the case of the CSNPs, no Pt growth was detected from the reaction at room temperature, whereas the reaction with the Sf-MON at 100 °C allowed additional deposition of Pt nanocrystals with an increased size of 2.1 (±0.3) nm compared to those obtained at 70 °C (Figure S2).

Consideration of the Pt Deposition Mechanism on the Mn_3O_4 Surface. These observations are reminiscent of galvanic replacement reactions, which have been previously reported between oxidizable metal substrates and reducible ions in the solution.[11,12] The spontaneous Pt deposition on Mn_3O_4 could be ascribed to the galvanic

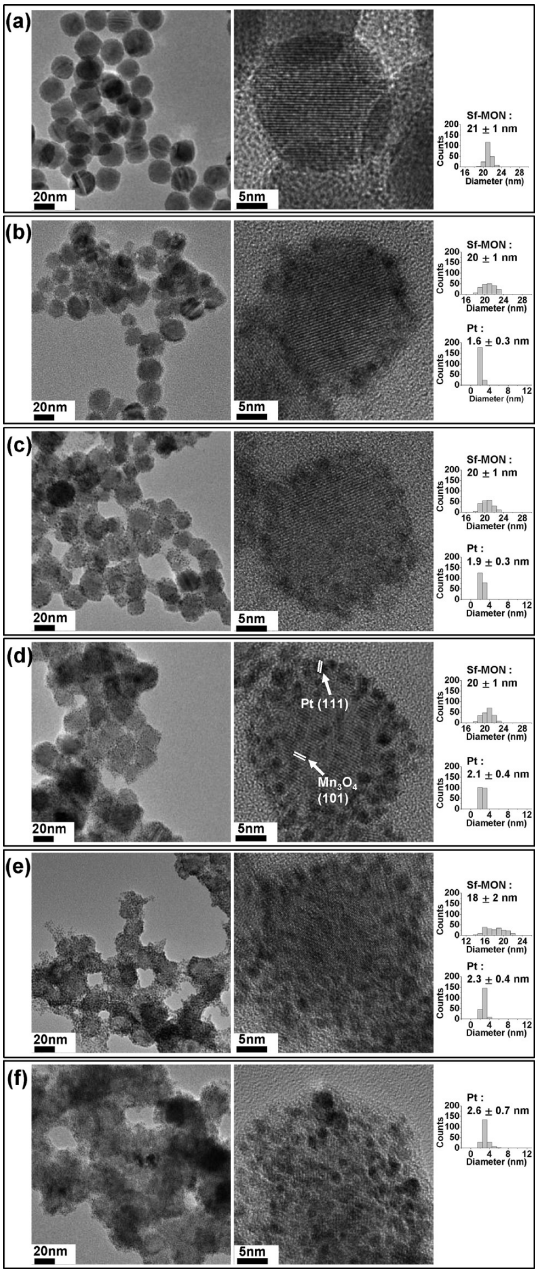

Figure 2. TEM, HRTEM, and size distribution histograms of (a) Sf-MON and PtMONC prepared by treating Sf-MON in a Na_2PtCl_4 solution for (b) 30 min, (c) 1 h, (d) 2 h, (e) 4 h, and (f) 14 h at 70 °C.

reactions in which $PtCl_4^{2-}$ ions are reduced to Pt(s) on the surface of Mn_3O_4 particles, while part of the Mn_3O_4 are oxidized and dissolved into the solution species. The plausibility of the galvanic reaction can be assessed based on the assumption that the process involves the following redox reactions along with their reduction potential values.

$$PtCl_4^{2-} + 2e^- \rightarrow Pt(s) + 4Cl^- \quad (1)$$

$$3Mn^{(III)}{}_2O_3(s) + 2H^+ + 2e^- \rightarrow 2Mn^{(II,\,III)}{}_3O_4(s) + H_2O \quad (2)$$

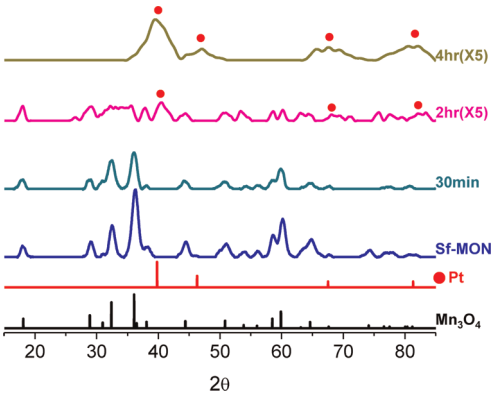

Figure 3. XRD patterns of Sf-MON and PtMONCs. XRD peaks corresponding to Mn_3O_4 and Pt are marked with green squares and red circles, respectively. The lines below show the position of the reflections corresponding to tetragonal Mn_3O_4 phase (JCPDS Card No. 24-0734) and the fcc Pt phase (JCPDS Card No. 87-0646).

The galvanic replacement reaction can be written by subtracting reaction 2 from reaction 1 as below:

$$PtCl_4^{2-} + 2Mn_3O_4(s) + H_2O \rightarrow Pt + 3Mn_2O_3(s) + 2H^+ + 4Cl^- \quad (3)$$

The reduction potentials of reactions 1 and 2 at pH = 2 are 0.758 and 0.712 V, respectively, which results in a slightly positive redox potential (*ca.* +0.046 V) of reaction 3.[27,28] Despite the positive redox potential of reaction 3, no noticeable Pt growth has been observed at room temperatures, which may be ascribed to the variation of the calculated redox potential value depending on the actual reaction conditions or kinetic barriers on surfaces. When the reaction temperature increases, the reduction potentials of the reaction 1 are known to increase,[28] whereas those of the reaction 2 decrease with a temperature coefficient of −1.26 mV/K.[29] Given the temperature dependence of reduction potentials, we expect that the redox potential of eq 3 at 70 °C is *ca.* +0.12 V, which is positive enough for the reaction 3 to proceed spontaneously despite the uncertainty in the actual reaction conditions. The role of the temperature was further confirmed by the control experiments, in which there was additional deposition of Pt nanocrystals with increased size at 100 °C compared to those obtained at 70 °C.

While the Pt growth on the Sf-MON was observed to accompany the diminution of Mn_3O_4, the presence of the further oxidized Mn_2O_3 phase was not detected by either XRD or X-ray photoelectron spectroscopy (XPS) analyses of the isolated PtMONCs. Therefore, the plausible overall reaction of the Pt deposition process can be suggested as follows, which includes either the *in situ* dissoution of Mn_2O_3 phases immediately upon their formation or the oxidative conversion of Mn_3O_4 phase directely into the soluble ionic species.

$$PtCl_4^{2-} + 2Mn_3O_4(s) + 16H^+ \rightarrow Pt(s) + 6Mn^{3+} + 4Cl^- + 8H_2O \quad (4)$$

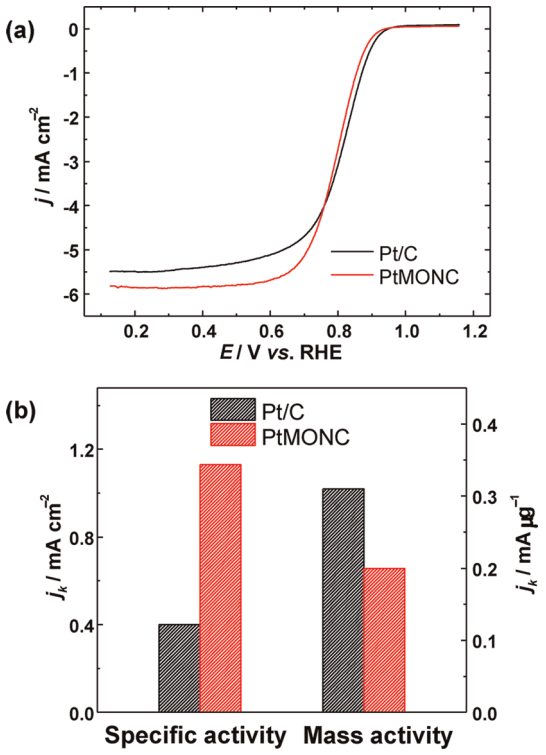

Figure 4. (a) ORR polarization curves for PtMONC (red) and Pt/C (black) obtained in a 0.1 M $HClO_4$ solution saturated with O_2 with a scan rate of 10 mV/s and a rotation rate of 1600 rpm. (b) Specific and mass activities for the catalysts at 0.85 V.

Among the control reactions carried out using other metal oxide nanoparticles instead of Mn_3O_4 nanoparticles, including Mn_2O_3, $MnFe_2O_4$, and Fe_3O_4 nanoparticles, the Pt growth was observed only in the reaction with $MnFe_2O_4$ nanoparticles, on the surfaces of which the conversion of the oxidation state from Mn^{2+} to Mn^{3+} is possible for the consequent reduction of $PtCl_4^{2-}$ to Pt(s) (Figure S3). While similar galvanic reactions between metal ions and metal substrates have been employed to deposit metal and fabricate hollow nanostructures, a galvanic replacement between metal oxide and metal ions has never been reported to the best of our knowledge.[11−17] Considering the ultrafine size and high density of the deposited Pt nanocrystals and the large surface area of the porous and nanoparticulate Mn_3O_4 support, a considerable amount of metal−metal oxide interfaces could be created through this deposition process. Therefore, the resulting hybrid nanostructure of the PtMONC leads us to expect improved performance in the catalytic application for which Pt-based materials are currently used.

Evaluation of Electrocatalytic Performance of Pt/Mn_3O_4 Nanocomposites. In order to verify the utility of the resulting PtMONC, we investigated its catalytic performance for the ORR, which is the rate-limiting reaction in the overall process of proton-exchange membrane fuel cells (PEMFCs).[30,31] Although carbon-supported Pt nanoparticles are currently used as cathode catalysts,

the commercialization of fuel cell technology still requires more advanced catalytic materials that enable a longer operation time with a much smaller amount of expensive Pt.[32,33] The activity of the PtMONC toward the ORR was evaluated by comparing it with that of commercial Pt/C catalysts (20 wt % Pt on carbon support, Alfa Aesar, HiSPEC fuel-cell grade). Figure 4a shows the ORR polarization curves obtained in O_2-saturated 0.1 M $HClO_4$ solutions on a glassy carbon rotating disk electrode (RDE) loaded with 7.02 $\mu g_{Pt}/cm^2_{disk}$ of each catalyst. The polarization curves indicate that the PtMONC catalysts exhibit electrocatalytic activity for the ORR that is fairly close to that of Pt/C catalysts, where the half-wave potential of the PtMONC catalysts is *ca.* 20 mV negatively shifted compared to that of Pt/C catalysts. To characterize the intrinsic electrocatalytic performance of the two catalysts, the kinetic current densities of the two catalysts during the ORR were evaluated and the respective specific and mass activities are compared in Figure 4b (Table S2 and Figure S4). The specific activity of the PtMONC was measured as being 2.8 times that of Pt/C catalysts. The electrochemical surface area (ECSA) of the Pt particles on the PtMONC is fairly small compared with that of the Pt particles on Pt/C; however, the electrochemically exposed Pt surfaces on the PtMONC are highly active for the ORR, which results in the higher specific activity of the PtMONC catalysts compared with that of Pt/C catalysts. Although the exact explanation requires further research, the enhancement in the specific activity might be attributed to the synergetic cocatalytic effect at the heterojunction interfaces formed between the Pt nanocrystal and the Mn_3O_4 support.[34,35] For example, Sun *et al.* reported the improved electrocatalytic activity of dumbbell-like Pt−Fe_3O_4 nanoparticles for the ORR, which was ascribed to the electronic structural change on Pt through the interactions between Pt and Fe_3O_4 in heterojunctions of the Pt−Fe_3O_4 structure.[21] The mass activity of the PtMONC catalysts was lower than that of Pt/C catalysts, when calculated based on the mass Pt in the catalysts, which may be attributable to the smaller ECSA per unit mass of Pt particles embedded on the surface of Mn_3O_4.

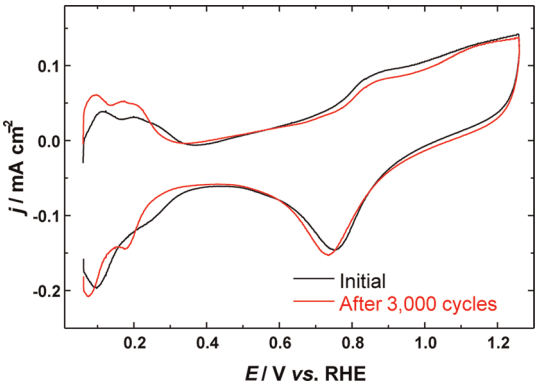

Figure 5. CVs of the PtMONC catalyst obtained before (black) and after (red) 3000 potential sweeps.

TABLE 1. Durability Test: Changes in ECSA (cm^2_{Pt}/cm^2_{disk}) after 3000 Cycles

	PtMONC	Pt/C
initial	1.82	5.91
after 3000 cycles	1.67	4.11
% change	− 8.2%	−30.5%

The durability of the Pt-based catalysts for the ORR is another critical issue to be overcome for the commercialization of PEMFC from an economic perspective.[36] The durability of the Pt-based catalysts is usually estimated by the loss of the ECSA during repetitive linear potential sweeps between 0.6 and 1.1 V at 50 mV/s in O_2-saturated 0.1 M $HClO_4$ solutions. Figure 5 shows the cyclic voltammograms (CVs) of PtMONC catalysts before and after 3000 potential sweeps. The ECSA for the PtMONC estimated from the charge associated with hydrogen adsorption indicates that there is a loss of 8.2% in ECSA after 3000 cycles (Table 1). The loss in ECSA for the PtMONC is less than that observed for Pt/C catalysts (30.5%). The loss of ECSA for Pt/C catalysts during the ORR has been reported to range from 30 to 60% over 3000 potential cycles.[37−39] The decrease in stability of Pt/C during the ORR can be ascribed to

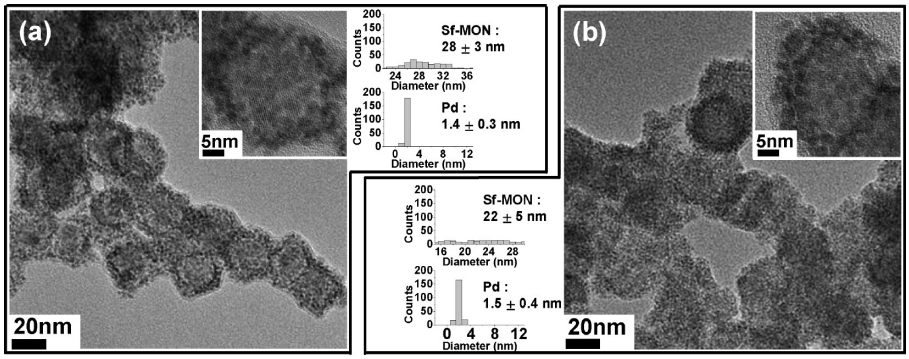

Figure 6. TEM images of PdMONC prepared by treating Sf-MON in a Na_2PdCl_4 solution for (a) 30 min and (b) 2 h at 70 °C.

the corrosion of the carbon support and Ostwald ripening/aggregation of Pt particles on the carbon support.[39−42] The enhanced ORR stability of the PtMONC can be ascribed to the strong metal support interaction between the Pt nanocrystals and the Mn_3O_4 support, which more effectively prevents the dissociation or the migration of the tightly bound Pt nanocrystals compared with that of the weakly interacting carbon support.[43,44] Although the detailed mechanism of the enhanced durability during the ORR should be investigated in the future, the development of the PtMONC suggests a possible new method of preparing more sustainable catalysts for cathodes in PEMFCs.

The current galvanic replacement-based protocol could also be applicable for depositing catalytic Pd nanoparticles, which have considerable potential for use in various organic reactions. The treatment of Sf-MONs with a Na_2PdCl_4 solution led to the formation of Pd nanoparticles on the Sf-MON surface, in a fashion similar to that observed in the Pt growth reaction, resulting in the formation of Pd/Mn_3O_4 nanocomposites (Figure 6 and Figure S5).

CONCLUSION

We realized the spontaneous deposition of Pt on the surface of Mn_3O_4 nanoparticles through a galvanic replacement process between Mn_3O_4 and $PtCl_4^{2-}$. The newly discovered process provides a simple protocol for producing catalytic nanocomposites, in which a high density of ultrafine Pt nanocrystals is dispersively immobilized on the surface of Mn_3O_4 nanoparticles. The higher specific activity and durability of the Pt/Mn_3O_4 nanocomposite as an electrocatalytic material for facilitating the ORR was demonstrated by comparison with the activity and durability of commercial Pt/C catalysts. The procedure explored in this study can be further developed as a generalized process that can be used to immobilize various metal catalysts on a metal oxide support, for realizing advanced catalytic systems with enhanced performance.

METHODS

General Consideration for the Synthesis. Any reagent including $MnCl_2 \cdot 4H_2O$ (Kanto), sodium oleate (TCI), 1-octadecene (Aldrich), Igepal CO-520 (Aldrich), tetraethyl orthosilicate (Acros), NH_4OH (Samchun chem.), NaOH (Samchun chem.), HCl (Samchun chem.), 1,2-distearoyl-*sn*-glycero-3-phosphoethanolamine-*N*-[methoxy-(polyethylene glycol)-2000] (Avanti Polar Lipids, Inc.), $Na_2PtCl_4 \cdot xH_2O$ (Strem), and $Na_2PdCl_4 \cdot xH_2O$ (Strem) was used as purchased without any purification. The analyses using transmission electron microscopy (TEM) were performed with JEOL JEM-2010. X-ray diffraction patterns were obtained using an X-ray diffractometer (18 kW) (Mac Science, Japan). Inductive coupling plasma atomic emission spectroscopy was carried out with direct-reading echelle ICP (LEEMAN).

Deposition of Pt Nanoparticles on CSNP. MnO−Mn_3O_4 core−shell nanoparticles (CSNPs) having an average size of 22 nm were prepared through a previously reported procedure.[23] The CSNPs (1 mg/mL) were mixed with 2 mL of $Na_2PtCl_4 \cdot xH_2O$ (7.5 mg/mL) aqueous solution and stirred at 70 °C for 2 h. After cooling to room temperature, the resulting solution was isolated by centrifugation and purified by repeating dispersion in an aqueous suspension and centrifugation three times.

Control Experiment with the Supernatant Solution Obtained after Etching CSNPs in a HCl Solution. MnO−Mn_3O_4 core−shell nanoparticles (CSNPs) having an average size of 22 nm were prepared through a previously reported procedure.[23] The pH of the CSNP solution was adjusted to be 5 using HCl solution. The solution was maintained at 70 °C for 2 h. After cooling to room temperature, the resulting solution was centrifuged; the supernatant and precipitate were separated. The $Na_2PtCl_4 \cdot xH_2O$ (7.5 mg/mL) aqueous solution was added to both the supernatant and precipitate. Each solution was stirred at 70 °C for 30 min. After cooling to room temperature, the resulting solution was isolated by centrifugation and then purified by repeating dispersion in an aqueous suspension and centrifugation three times.

Preparation of Sf-MON. Oleic acid stabilized the MnO nanoparticles (22 nm in size), and these nanoparticles were coated with a SiO_2 shell through a previously reported procedure.[22,45] The MnO nanoparticles encapsulated by the SiO_2 shell were thermally transformed into Mn_3O_4 by annealing 100 mg of SiO_2 nanospheres encapsulating the MnO nanoparticles under air at 500 °C for 5 h. The annealed solids were dispersed in a degassed NaOH solution (3.0 M, pH 14.0) and stirred at room temperature under the N_2 atmosphere for 15 h to remove the silica shell. The resulting solids, Sf-MON, were collected by centrifugation and washed with water by repeating dispersion in an aqueous suspension and centrifugation three times.

Deposition of Pt Nanoparticles on Sf-MON (Synthesis of PtMON). Twenty milliliters of the Na_2PtCl_4 solution (7.5 mg/mL) was added to 10 mL of an aqueous suspension containing Sf-MON (3 mg/mL) at 70 °C and gently stirred for 2 h. After cooling to room temperature, the resulting PtMONC was isolated by centrifugation and purified by repeating dispersion in an aqueous suspension and centrifugation three times. For determining the Mn and Pt contents of the nanoparticles, 1 mL of the suspensions was taken from the Pt growth reaction suspension at different reaction times (30 min, 1 h, 4 h, and 14 h) and the solids were isolated by centrifugation. The obtained solids were completely dissolved with aqua regia, and the Mn and Pt contents were determined by ICP-AES analysis.

Control Experiments with Surfactant-Free Mn_2O_3, $MnFe_2O_4$, and Fe_3O_4 Nanoparticles. Mn_2O_3 nanoparticles in a surfactant-free state were prepared through a reported procedure.[46] Oleic-acid-stabilized $MnFe_2O_4$ and Fe_3O_4 nanoparticles were synthesized through a reported thermal decomposition method.[47] Then, the surfactant-free $MnFe_2O_4$ and Fe_3O_4 nanoparticles were prepared through the same solid-state transformation procedure that was applied for the synthesis of Sf-MON. The Pt growth reactions were carried out in a similar procedure as that for the synthesis of PtMON, except for the use of the surfactant-free Mn_2O_3, $MnFe_2O_4$, and Fe_3O_4 nanoparticles instead of Sf-MONs.

Reagents and Instruments for the Electrochemical Study. All solutions were prepared using purified water (Milli-Q, 18.2 MW·cm). All reagents, including Pt/C catalysts (20 wt % Pt on carbon support, Alfa Aesar, HiSPEC fuel-cell grade), Nafion solution (Sigma), and $HClO_4$ (Merck), were used as purchased without any purification, and 0.1 M $HClO_4$ was used as a supporting electrolyte solution. Electrochemical measurements were performed using a CHI 400A (CH Instrument) potentiostat. A Pt wire and Ag/AgCl electrodes (3 M KCl) were used as the counter and reference electrodes, respectively. A glassy carbon rotating disk electrode (GCRDE, $d = 5$ mm, Pine Instrumentation) was used as a working electrode. The rotating disk electrode data for ORR polarization curves were obtained using a Pine Model MSRX rotator.

Electrode Preparation. An aqueous dispersion of Pt/C (0.30 mg/mL) or PtMONC (0.15 mg/mL) catalyst was sonicated for 15 min. A portion of the dispersion (23 μL for Pt/C and 20 μL for PtMONC) was then dropped onto the GCRDE (A = 0.196 cm^2), which corresponds to a Pt metal loading of 7.02 μg/cm^2. After drying under air for 2 h, the electrode was covered with 15 μL Nafion solution (0.05%), followed by the evaporation of water and vacuum treatment for 30 min prior to the electrochemical measurement.

Electrochemical Measurements. The ORR polarization curves were obtained using O_2-saturated 0.1 M $HClO_4$ electrolyte solutions using the catalyst-loaded GC RDEs, at a rotation rate of 1600 rpm and a scan rate of 10 mV/s. Before obtaining the ORR polarization curves, the electrode was subjected to several potential cycling steps between −0.06 and 1.26 V to clean the electrode surface. For evaluating the mass and specific activities, the kinetic currents (i_k) were calculated from the ORR polarization curves using the mass-transport correction equation for a rotating disk electrode:[33]

$$i_k = \frac{i_d \times i}{i_d - i}$$

where i is the observed current at 0.85 V and i_d corresponds to the diffusion-limited current. The calculated kinetic current is normalized to the loading amount of the metal and electrochemically active surfaces area (ECSA) for evaluating the mass and specific activity, respectively. For the ECSA evaluation, cyclic voltammograms were obtained using N_2-saturated 0.1 M $HClO_4$ electrolyte solutions, at a scan rate of 50 mV/s (Figure S5), and the ECSA was estimated from the charge under hydrogen adsorption.[48]

Conflict of Interest: The authors declare no competing financial interest.

Acknowledgment. This work was supported by the National Research Foundation of Korea (NRF) grant funded by the Korea government (MEST) 2011-0017377 (I.S.L.) and 2010-0004126 (J.K.)

Supporting Information Available: More experimental data including TEM images, CVs, ICP-AES data, and electrochemical data (Figures S1−S5, Tables S1 and S2). This material is available free of charge *via* the Internet at http://pubs.acs.org.

REFERENCES AND NOTES

1. Zhou, B.; Han, S.; Raja, R.; Somorjai, G. A. *Nanotechnology in Catalysis*; Springer: New York, 2007; Vol. 3.
2. Astruc, D.; Lu, F.; Aranzaes, J. R. Nanoparticles as Recyclable Catalysts: The Frontier between Homogeneous and Heterogeneous Catalysis. *Angew. Chem., Int. Ed.* **2005**, *44*, 7852–7872.
3. Cao, A.; Luc, R.; Veser, G. Stabilizing Metal Nanoparticles for Heterogeneous Catalysis. *Phys. Chem. Chem. Phys.* **2010**, *12*, 13499–13510.
4. Campelp, J. M.; Luna, D.; Luque, R.; Marinas, J. M.; Romero, A. A. Sustainable Preparation of Supported Metal Nanoparticles and Their Applications in Catalysis. *ChemSusChem* **2009**, *2*, 18–45.
5. Farmer, J. A.; Campbell, C. T. Ceria Maintains Smaller Metal Catalyst Particles by Strong Metal-Support Bonding. *Science* **2010**, *329*, 933–936.
6. Lee, Y.; Garcia, M. A.; Frey Huls, N. A.; Sun, S. Synthetic Tuning of the Catalytic Properties of Au-Fe_3O_4 Nanoparticles. *Angew. Chem., Int. Ed.* **2010**, *49*, 1271–1274.
7. Herzing, A. A.; Kiely, C. J.; Carley, A. F.; Landon, P.; Hutchings, G. J. Identification of Active Gold Nanoclusters on Iron Oxide Supports for CO Oxidation. *Science* **2008**, *321*, 1331–1335.
8. Comotti, M.; Li, W.-C.; Spliethoff, B.; Schüth, F. Support Effect in High Activity Gold Catalysts for CO Oxidation. *J. Am. Chem. Soc.* **2006**, *128*, 917–924.
9. Chen, M. S.; Goodman, D. W. The Structure of Catalytically Active Gold on Titania. *Science* **2004**, *306*, 252–255.
10. Haruta, M. Catalysis of Gold Nanoparticles Deposited on Metal Oxides. *CATTECH* **2002**, *6*, 102–115.
11. Sun, Y. Metal Nanoplates on Semiconductor Substrates. *Adv. Funct. Mater.* **2010**, *20*, 3646–3657.
12. Sun, Y.; Mayers, B.; Xia, Y. Metal Nanostructures with Hollow Interiors. *Adv. Mater.* **2003**, *15*, 641–646.
13. Habas, S. E.; Yang, P.; Mokari, T. Selective Growth of Metal and Binary Metal Tips on CdS Nanorods. *J. Am. Chem. Soc.* **2008**, *130*, 3294–3295.
14. Yin, Y.; Erdonmez, C.; Aloni, S.; Alivisatos, A. P. Faceting of Nanocrystals during Chemical Transformation: From Solid Silver Spheres to Hollow Gold Octahedra. *J. Am. Chem. Soc.* **2006**, *128*, 12671–12673.
15. Aizawa, M.; Cooper, A. M.; Malac, M.; Buriak, J. M. Silver Nano-Inukshuks on Germanium. *Nano Lett.* **2005**, *5*, 815–819.
16. Mokari, T.; Rothenberg, E.; Popov, I.; Costi, R.; Banin, U. Selective Growth of Metal Tips onto Semiconductor Quantum Rods and Tetrapods. *Science* **2004**, *304*, 1787–1790.
17. Sun, Y.; Xia, Y. Shape-Controlled Synthesis of Gold and Silver Nanoparticles. *Science* **2002**, *298*, 2176–2179.
18. Anumol, E. A.; Kundu, P.; Deshpande, P. A.; Madras, G.; Ravishankar, N. New Insights into Selective Heterogeneous Nucleation of Metal Nanoparticles on Oxides by Microwave-Assisted Reduction: Rapid Synthesis of High-Activity Supported Catalysts. *ACS Nano* **2011**, *5*, 8049–8061.
19. Palchoudhury, S.; Xu, Y.; Goodwinb, J.; Bao, Y. Synthesis of Multiple Platinum-Attached Iron Oxide Nanoparticles. *J. Mater. Chem.* **2011**, *21*, 3966–3970.
20. Zhou, H.-P.; Wu, H.-S.; Shen, J.; Yin, A.-X.; Sun, L.-D.; Yan, C.-H. Thermally Stable Pt/CeO_2 Hetero-nanocomposites with High Catalytic Activity. *J. Am. Chem. Soc.* **2010**, *132*, 4998–4999.
21. Wang, C.; Daimon, H.; Sun, S. Dumbbell-like Pt-Fe_3O_4 Nanoparticles and Their Enhanced Catalysis for Oxygen Reduction Reaction. *Nano Lett.* **2009**, *9*, 1493–1496.
22. Anisur, R. M.; Shin, J. M.; Choi, H. H.; Yeo, K. M.; Kang, E. J.; Lee, I. S. Hollow Silica Nanosphere Having Functionalized Interior Surface with Thin Manganese Oxide Layer: Nanoreactor Framework for Size-selective Lewis Acid Catalysis. *J. Mater. Chem.* **2010**, *20*, 10615–10621.
23. Shin, J. M.; Anisur, R. M.; Ko, M. K.; Im, G. H.; Lee, J. H.; Lee, I. S. Hollow Manganese Oxide Nanoparticles as Multifunctional Agents for Magnetic Resonance Imaging and Drug Delivery. *Angew. Chem., Int. Ed.* **2009**, *48*, 321–324.
24. Chen, A.; Holt-Hindle, P. Platinum-Based Nanostructured Materials: Synthesis, Properties, and Applications. *Chem. Rev.* **2010**, *110*, 3767–3804.
25. Shin, J.; Ha, T.; Lee, I. S. Generation of Hollow $MnSiO_3$ Nanostructures through the Solid-State Reaction of Mn_3O_4 and Pd/PdO Nanocrystals Dimensionally Confined within Nanosized Silica Spheres. *Eur. J. Inorg. Chem.* **2010**, 357–360.
26. Shin, J.; Kim, H.; Lee, I. S. Synthesis of Fe_3O_4/PdO Heterodimer Nanocrystals in Silica Nanospheres and Their Controllable Transformation into Fe_3O_4/Pd Heterodimers and FePd Nanocrystals. *Chem. Commun.* **2008**, 5553–5555.
27. Bard, A. J.; Parsons, R.; Jordan, J. *Standard Potentials in Aqueous Solution*; CRC Press: New York, 1985.
28. Ginstrup, O. The Redox System Platinum(0)/Platinum(II)/Platinum(IV) with Chloro and Bromo Ligands. *Acta Chem. Scand.* **1972**, *26*, 1527–1541.
29. Bratsch, S. G. Standard Electrode Potentials and Temperature Coefficients in Water at 298.15 K. *J. Phys. Chem. Ref. Data* **1989**, *18*, 1–21.
30. Ho, V. T. T.; Pan, C.-J.; Rick, J.; Su, W.-N.; Hwang, B.-J. Nanostructured $Ti_{0.7}Mo_{0.3}O_2$ Support Enhances Electron Transfer to Pt: High-Performance Catalyst for Oxygen Reduction Reaction. *J. Am. Chem. Soc.* **2011**, *133*, 11716–11724.
31. Subban, C. V.; Zhou, Q.; Hu, A.; Moylan, T. E.; Wagner, F. T.; DiSalvo, F. J. Sol−Gel Synthesis, Electrochemical Characterization, and Stability Testing of $Ti_{0.7}W_{0.3}O_2$ Nanoparticles for Catalyst Support Applications in Proton-Exchange Membrane Fuel Cells. *J. Am. Chem. Soc.* **2010**, *132*, 17531–17536.
32. de Bruijn, F. A.; Dam, V. A. T.; Janssen, G. J. M. Review: Durability and Degradation Issues of PEM Fuel Cell Components. *Fuel Cells* **2008**, *8*, 3–22.

33. Gasteiger, H. A.; Kocha, S. S.; Sompalli, B.; Wagner, F. T. Activity Benchmarks and Requirements for Pt, Pt-Alloy, and Non-Pt Oxygen Reduction Catalysts for PEMFCs. *Appl. Catal. B* **2005**, *56*, 9–35.
34. El-Deab, M. S.; Ohsaka, T. Manganese Oxide Nanoparticles Electrodeposited on Platinum Are Superior to Platinum for Oxygen Reduction. *Angew. Chem., Int. Ed.* **2006**, *45*, 5963–5966.
35. Xu, C.; Tian, Z.; Shen, P.; Jiang, S. P. Oxide (CeO_2, NiO, Co_3O_4 and Mn_3O_4)-Promoted Pd/C Electrocatalysts for Alcohol Electrooxidation in Alkaline Media. *Electrochim. Acta* **2008**, *53*, 2610–2618.
36. Shao, Y.; Yin, G.; Gao, Y. Understanding and Approaches for the Durability Issues of Pt-Based Catalysts for PEM Fuel Cell. *J. Power Sources* **2007**, *171*, 558–566.
37. Sun, S.; Zhang, G.; Geng, D.; Chen, Y.; Li, R.; Cai, M.; Sun, X. A Highly Durable Platinum Nanocatalyst for Proton Exchange Membrane Fuel Cells: Multiarmed Starlike Nanowire Single Crystal. *Angew. Chem., Int. Ed.* **2011**, *50*, 422–426.
38. Lim, B.; Jiang, M.; Camargo, P. H. C.; Cho, E. C.; Tao, J.; Lu, X.; Zhu, Y.; Xia, Y. Pd—Pt Bimetallic Nanodendrites with High Activity for Oxygen Reduction. *Science* **2009**, *324*, 1302–1395.
39. Lim, B.; Lu, X.; Jiang, M.; Camargo, P. H. C.; Cho, E. C.; Lee, E. P.; Xia, Y. Facile Synthesis of Highly Faceted Multioctahedral Pt Nanocrystals through Controlled Overgrowth. *Nano Lett.* **2008**, *8*, 4043–4047.
40. Wang, H.-H.; Zhou, Z.-Y.; Yuan, Q.; Tian, N.; Sun, S.-G. Pt Nanoparticle Netlike-Assembly as Highly Durable and Highly Active Electrocatalyst for Oxygen Reduction Reaction. *Chem. Commun.* **2011**, *47*, 3407–3409.
41. Shao-Horn, Y.; Sheng, W. C.; Chen, S.; Ferreira, P. J.; Holby, E. F.; Morgan, D. Instability of Supported Platinum Nanoparticles in Low-Temperature Fuel Cells. *Top. Catal.* **2007**, *46*, 285–305.
42. Ferreira, P. J.; la O', G. J.; Shao-Horn, Y.; Morgan, D.; Makharia, R.; Kocha, S.; Gasteiger, H. A. Instability of Pt/C Electrocatalysts in Proton Exchange Membrane Fuel Cells. *J. Electrochem. Soc.* **2005**, *152*, A2256–A2271.
43. Qin, Z.-H.; Lewandowski, M.; Sun, Y.-N.; Shaikhutdinov, S.; Freund, H.-J. Encapsulation of Pt Nanoparticles as a Result of Strong Metal—Support Interaction with Fe_3O_4 (111). *J. Phys. Chem. C* **2008**, *112*, 10209–10213.
44. Huang, S.-Y.; Ganesan, P.; Park, S.; Popov, B. N. Development of a Titanium Dioxide-Supported Platinum Catalyst with Ultrahigh Stability for Polymer Electrolyte Membrane Fuel Cell Applications. *J. Am. Chem. Soc.* **2009**, *131*, 13898–13899.
45. Na, H. B.; Lee, J. H.; An, K.; Park, Y. I.; Park, M.; Lee, I. S.; Nam, D.-H.; Kim, S. T.; Kim, S.-H.; Kim, S.-W.; *et al.* Development of a T_1 Contrast Agent for Magnetic Resonance Imaging Using MnO Nanoparticles. *Angew. Chem., Int. Ed.* **2007**, *46*, 5397–5401.
46. Gnanam, S.; Rajendran., V. Synthesis of CeO_2 or α-Mn_2O_3 Nanoparticles *via* Sol—Gel Process and Their Optical Properties. *J. Sol—Gel Sci. Technol.* **2011**, *58*, 62–69.
47. Park, J.; An, K.; Hwang, Y.; Park, J.-G.; Noh, H.-J.; Kim, J.-Y.; Park, J.-H.; Hwang, N.-M.; Hyeon, T. Ultra-Large-Scale Syntheses of Monodisperse Nanocrystals. *Nat. Mater.* **2004**, *3*, 891–895.
48. Trasatti, S.; Petrii, O. A. Real Surface Area Measurements in Electrochemistry. *Pure Appl. Chem.* **1991**, *63*, 711–734.